Letter

Probing QCD critical point and induced gravitational wave by black hole physics

Rong-Gen Cai,[2,3,*] Song He,[1,4,†] Li Li,[2,3,5,‡] and Yuan-Xu Wang[1,§]

[1]*Center for Theoretical Physics and College of Physics, Jilin University, Changchun 130012, People's Republic of China*

[2]*CAS Key Laboratory of Theoretical Physics, Institute of Theoretical Physics, Chinese Academy of Sciences, Beijing 100190, China*

[3]*School of Fundamental Physics and Mathematical Sciences, Hangzhou Institute for Advanced Study, UCAS, Hangzhou 310024, China*

[4]*Max Planck Institute for Gravitational Physics (Albert Einstein Institute), Am Mühlenberg 1, 14476 Golm, Germany*

[5]*Peng Huanwu Collaborative Center for Research and Education, Beihang University, Beijing 100191, China*

(Received 14 January 2022; revised 26 September 2022; accepted 22 November 2022; published 13 December 2022)

Locating the critical endpoint of QCD and the region of a first-order phase transition at finite baryon chemical potential is an active research area for QCD matter. We provide a gravitational dual description of QCD matter at finite baryon chemical potential μ_B and finite temperature using the nonperturbative approach from gauge/gravity duality. After fixing all model parameters using state-of-the-art lattice QCD data at zero chemical potential, the predicted equations of state and QCD trace anomaly relation are in quantitative agreement with the latest lattice results. We then give the exact location of the critical endpoint as well as the first-order transition line, which is within the coverage of many upcoming experimental measurements. Moreover, using the data from our model at finite μ_B, we calculate the spectrum of the stochastic gravitational wave background associated with the first-order QCD transition in the early Universe, which could be observable via pulsar timing in the future.

DOI: 10.1103/PhysRevD.106.L121902

I. INTRODUCTION

As one of the most interesting and fundamental challenges of high-energy physics, the phase diagram of QCD has been intensively studied. It involves the behavior of strongly interacting matter under extreme conditions [1–3], ranging from cosmology and astrophysics to heavy-iron collisions. Due to the strong interaction in the nonperturbative regime, it has not been possible to obtain the full QCD phase diagram directly from QCD in terms of the temperature T and the baryon chemical potential μ_B or the baryon number density n_B. While lattice QCD can provide reliable first-principles information at zero density [4–6], it fails at finite density due to the famous sign problem [2]. Note, however, that the lattice data can be extrapolated to finite μ_B via different systematical schemes [7–9], but this is only reliable for small μ_B. Meanwhile, many effective low-energy models have been proposed to study the QCD phase diagram under certain conditions, such as [10–12], for which it is difficult to match the lattice QCD data quantitatively. Nevertheless, the QCD matter is now believed to be in a hadronic phase of color-neutral bound states at low T and small μ_B, while it is deconfined at high T and large μ_B, known as the quark-gluon plasma. These two phases are separated by a transition at small μ_B and are expected to change into a first-order transition for higher μ_B. The critical point between them is the QCD critical endpoint (CEP), which has been under active investigation by experiments and theoretical calculations.

On the other hand, the gauge/gravity duality [13–16] provides a powerful nonperturbative approach to solving the strongly coupled non-Abelian gauge theories by mapping to a weakly coupled gravitational system with one higher dimension. In particular, it provides a convenient way to incorporate real-time dynamics and transport properties at

*cairg@itp.ac.cn
†Corresponding author.
hesong@jlu.edu.cn
‡Corresponding author.
liliphy@itp.ac.cn
§yuanxu20@mails.jlu.edu.cn

finite temperatures and densities. Previous studies (e.g., [17–21]) have provided a strong indication that holography can make quantitative description of the properties of QCD in the nonperturbative regime. The construction of the QCD phase diagram in such a holographic approach was initiated by [22,23], where the Einstein-Maxwell-dilaton (EMD) theory was used to mimic properties in the QCD phase diagram. Since then, several attempts have been made toward the direction of the phase diagram in the $T-\mu_B$ plane (see e.g., [24–32]). In the spirit of effective field theory, the model parameters of the bulk gravitational theory should be fixed by matching with lattice QCD results. Therefore, it is crucial to use up to date lattice simulation for reliable prediction at finite μ_B.

In this paper we construct a holographic QCD (hQCD) model in which all parameters are fixed using state-of-the-art lattice QCD data [6] at $\mu_B = 0$, generated by highly improved stagger fermion action. Moreover, all thermodynamic quantities are computed directly from the holographic renormalization and the so-called thermodynamic consistency relations [33]. Our prediction for the thermodynamic observables at finite μ_B is in quantitative agreement with the latest lattice results that are available for $\mu_B/T < 3.5$ [9]. We also calculate both the chiral and gluon condensates. Remarkably, we show for the first time in holography that the gluon condensate agrees with the lattice simulation regarding the QCD conformal anomaly. We then manage to make precise predictions for the QCD phase diagram at finite μ_B, in particular a first-order line and a CEP located at $T_C = 105$ MeV and $\mu_C = 555$ MeV. Interestingly, the location of our CEP can be checked in the near future by many important upcoming facilities. Moreover, the strong first-order phase transition (SFOPT) in the early universe is an important source of the stochastic gravitational wave (GW) background (see, e.g., [38–41] and references therein). While various scenarios of new physics beyond the Standard Model of particle physics have been considered to engineer an SFOPT in the literature, our present model provides a scenario for phase transition GWs within the Standard Model.

II. HOLOGRAPHIC MODEL

We begin with the five-dimensional EMD theory

$$S = \frac{1}{2\kappa_N^2}\int d^5x\sqrt{-g}\left[\mathcal{R} - \frac{1}{2}\nabla_\mu\phi\nabla^\mu\phi - \frac{Z(\phi)}{4}F_{\mu\nu}F^{\mu\nu} - V(\phi)\right], \tag{1}$$

with a minimal set of fields for capturing the essential dynamics. Here κ_N^2 is the effective Newton constant. In addition to the metric $g_{\mu\nu}$ that characterizes the geometry, the real scalar ϕ (known as a dilaton) encodes the running of the gauge coupling, and the Maxwell field A_μ accounts for a finite baryon density. $Z(\phi)$ and $V(\phi)$ are two phenomenological terms that will be fixed by matching to the lattice QCD at $\mu_B = 0$.

The hairy black hole reads

$$ds^2 = -f(r)e^{-\eta(r)}dt^2 + \frac{dr^2}{f(r)} + r^2dx_3^2,$$
$$\phi = \phi(r), \qquad A_t = A_t(r), \tag{2}$$

where $dx_3^2 = dx^2 + dy^2 + dz^2$ and r is the holographic radial coordinate with the asymptotical anti–de Sitter (AdS) boundary at $r \to \infty$. Denoting the event horizon as r_h at which f vanishes, the temperature and entropy density can be obtained as

$$T = \frac{1}{4\pi}f'(r_h)e^{-\eta(r_h)/2}, \qquad s = \frac{2\pi}{\kappa_N^2}r_h^3, \tag{3}$$

while the baryon chemical potential μ_B and density n_B can be obtained from A_t at the AdS boundary, we read the energy density ϵ and pressure P directly by the dual stress-energy tensor via the holographic renormalization [42,43]. We refer to the Supplemental Material for more details [44]. Then, the equation of state (EOS) and transport properties can be determined precisely. The form of V and Z is partially motivated by the one in [17,22,23], although these models were not able to simultaneously fit the lattice data for equilibrium and near-equilibrium features quantitatively.

By global fitting the state-of-the-art lattice data [6,9] with $(2+1)$-flavors at zero net-baryon density (see Fig. 1), the hQCD model can be fixed to be

$$V(\phi) = -12\cosh[c_1\phi] + \left(6c_1^2 - \frac{3}{2}\right)\phi^2 + c_2\phi^6,$$
$$\kappa_N^2 = 2\pi(1.68), \qquad \phi_s = 1085\ \text{MeV},$$
$$Z(\phi) = \frac{1}{1+c_3}\operatorname{sech}[c_4\phi^3] + \frac{c_3}{1+c_3}e^{-c_5\phi}, \tag{4}$$

with $c_1 = 0.7100$, $c_2 = 0.0037$, $c_3 = 1.935$, $c_4 = 0.085$, $c_5 = 30$. Here $\phi_s = r\phi|_{r\to\infty}$ is the source term of the scalar field ϕ, which essentially breaks the conformal symmetry and plays the role of the energy scale. The fitting results are presented in the upper panel of Fig. 1. In addition to the EOS, the specific heat $C_V = (d\epsilon/dT)_{\mu_B}$, and the second-order baryon susceptibility $\chi_2^B = (dn_B/d\mu_B)_T/T^2$ at zero density, which are important quantities characterizing QCD transition, agree with the lattice data quantitatively.

Given the local bulk description of QCD (4), we also calculate the gluon condensate and the condensates for u, d, s quarks in the spirit of the Karch-Katz-Son-Stephano model [45] by introducing appropriate probe actions. The temperature dependence of these condensates is in quantitative agreement with the lattice simulations [6], see the lower panel of Fig. 1. Remarkably, the trace anomaly

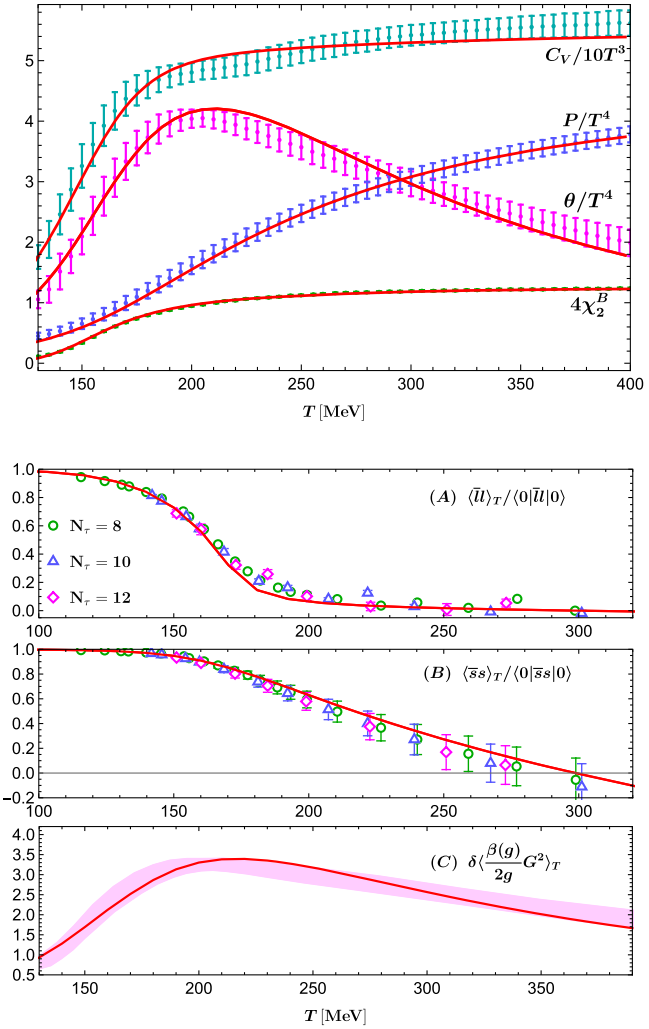

FIG. 1. Thermodynamics and condensates at $\mu_B = 0$. Upper panel: The pressure P, the trace anomaly $\theta \equiv \epsilon - 3P$, the specific heat C_V, and the baryon susceptibility χ_2^B. Lower panel: The condensates for (A) the u, d quarks, (B) the s quark, and (C) the gluon. Data with error bars and the pink band are from lattice QCD [6,9], while solid red curves are from our hQCD model. N_τ is the temporal extent in lattice QCD. Following lattice QCD notations, the condensates of the light ($l = u, d$) quarks and the s quark are normalized by there values at zero temperature. The gluon condensate $\langle\frac{\beta(g)}{2g}G^2\rangle_T$ is subtracted by its vacuum value, where $\beta(g)$ is the β-function and g is QCD gauge coupling.

$(\epsilon - 3P)$ is found to be consistent with the summation of the quark and gluon condensates. It is the first time that this relation is realized in a holographic setup (see the Supplemental Material [44] for technical details).

So far, our holographic model is completely fixed, and there are no free parameters. In Fig. 2, we compare the holographic results with the latest lattice QCD [9] which combines the Taylor-expanded approach and the analytical continuation approach. The holographic predictions are in quantitative agreement with the lattice results available for small chemical potentials, which strongly supports our hQCD model.

III. QCD PHASE DIAGRAM

Having completely fixed the holographic model, we can now construct the phase diagram in the $T - \mu_B$ plane by numerically solving a series of black holes. We find that, as μ_B increases, the crossover on the T-axis is sharpened into a first-order line at the CEP (see Fig. 3). Since the transition from $\mu_B = 0$ up to the CEP is a smooth crossover, there is no unique way to determine the transition temperature in the literature. Some suitable probes characterizing the drastic change of degrees of freedom between the quark-gluon plasma (QGP) and the hadron resonances gas are the minimum of the speed of sound c_s and the maximum increasing point of χ_2^B. The transition lines of the two probes are shown in Fig. 3. The transition temperatures of the probes at zero μ_B compare well with the predictions of lattice QCD for the same up to the quark-hadron transition region around 140–160 MeV [46–48]. Although they do not coincide quantitatively in the crossover region, they show similar behavior and are in the same order of magnitude. Moreover, they come together at the critical point μ_C.

For a baryon chemical potential above μ_C, the QCD transition becomes a first-order transition for which the free energy can uniquely determine the transition point from the holographic calculation (see the solid black line in Fig. 3). The first-order line decreases monotonically with μ_B. Although we cannot see when the line will terminate, our numerics suggest that the transition temperature becomes significantly small, approximately larger than $\mu_B \sim 1050$ MeV, beyond which no stable black holes have been found. In this region, color superconductivity or related phenomena might be set in.

The CEP predicted by our hQCD model is located at $T_C = 105$ MeV, $\mu_C = 555$ MeV (the red dot in Fig. 3). Therefore, there is no first-order phase transition in the region with $\mu_B/T < \mu_C/T_C \approx 5.3$, which is consistent with the thermodynamics of Fig. 2. We also show the location of CEP from different models and note that the current best lattice estimate suggests that CEP is likely above $\mu_B \sim 300$ MeV [61,62]. The variation in priorities is considerable, but most of them are close to the transition line we found. Moreover, compared to other predictions, our CEP is close to those obtained by the Schwinger-Dyson equation [53,54] or the functional renormalization group [57], respectively. Nevertheless, all our predictions are at least qualitatively consistent with the consensus expectations for the QCD phase diagram. Interestingly, the predicted location of CEP is within the coverage of the STAR fixed target program (FXT) and future (FAIR [63,64], JPARC-HI and NICA [65]) experimental facilities [60]. Therefore, our prediction can be verified in the near future.

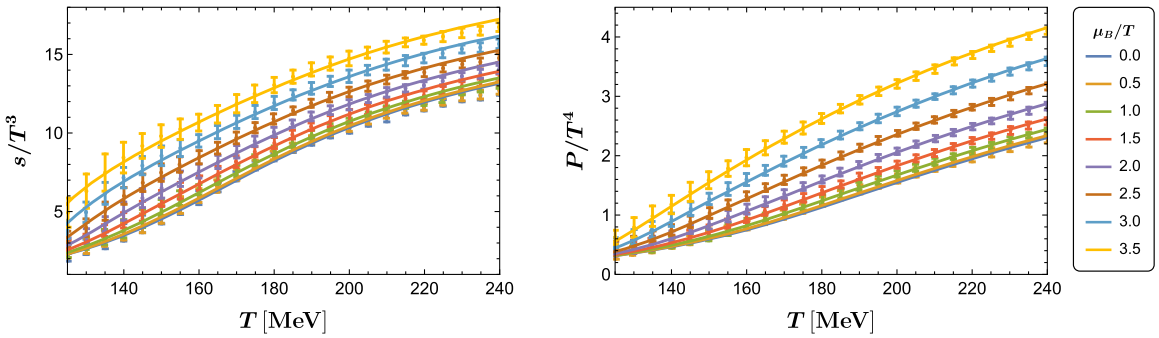

FIG. 2. The entropy density s (left) and the pressure P (right) at small chemical potentials. Our holographic computations (solid curves) are compared with the latest lattice QCD results from [9].

IV. GRAVITATIONAL WAVES FROM QCD PHASE TRANSITION

An important feature associated with the first order QCD transition in the early universe is the generation of a stochastic background of GWs, for which bubbles of the broken phase nucleate and expand in the presence of a plasma background of false vacuum. The GWs can be generated in three processes; bubble collisions, sound waves, and magnetohydrodynamic turbulence. Some preliminary studies of the GW spectra from holographic QCD have been summarized in [66]. It has been recognized that higher-order corrections prevent true runaway transitions from occurring [67], thus the bubble wall terminal velocity $v_w < 1$. For these nonrunway bubbles, the GWs will be dominated by sound waves for which the energy spectrum reads [68]

$$h^2\Omega_{GW}(f) = 8.5\times10^{-6}\left(\frac{100}{g_n}\right)^{1/3}\left(\frac{H_n}{\beta}\right)\left(\frac{\kappa\alpha}{1+\alpha}\right)^2 \times v_w\left(\frac{f}{f_{SW}}\right)^3\left[\frac{7}{4+3(f/f_{SW})^2}\right]^{7/2}, \tag{5}$$

with the peak frequency

$$f_{SW} = 1.9\times10^{-8}\left(\frac{1}{v_w}\right)\left(\frac{\beta}{H_n}\right)\left(\frac{T_n}{100\ \text{Mev}}\right)\left(\frac{g_n}{100}\right)^{1/6}\ \text{Hz}. \tag{6}$$

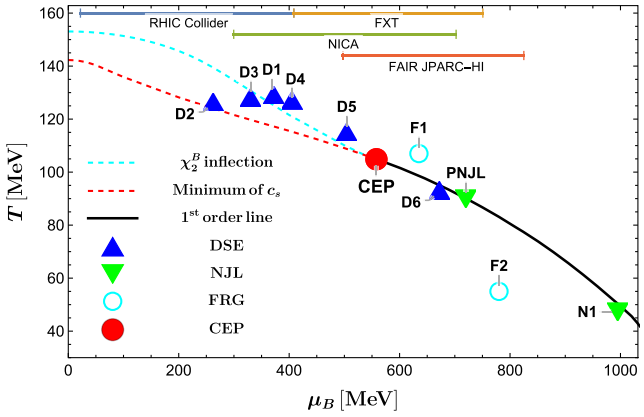

FIG. 3. The QCD phase diagram predicted from our model. The minimum of c_s and the maximally increasing point of the χ_2^B are denoted by dashed red and cyan lines, respectively. The first-order phase transition line (solid black line) is determined by free energy. Our result for the location the CEP is $T_C = 105$ MeV, $\mu_C = 555$ MeV (bold red dot). The CEP obtained by different approaches are presented as well, including the Schwinger-Dyson equation (DSE), the Nambu-Jona-Lasinio model (NJL), and the functional renormalization group (FRG). DSE: D1-D6 are from [49–54]. NJL: PNJL is from [55] and NJL1 from [56]. FRG: F1-F2 are from [57,58]. The coverage of RHIC [59], the STAR fixed target program (FXT), and future (FAIR, JPARC-HI, and NICA) experimental facilities [60] is also indicated at the top of the figure.

The strength of the GW spectrum depends on many parameters that can be obtained from our holographic model. We discuss each of these quantities in turn.

T_n is approximated by the critical temperature of the first-order transition, see the solid black line in Fig. 3. Beyond the bag model approximation, the phase transition strength α is given by [39]

$$\alpha = \left.\frac{\theta_+ - \theta_-}{3w_+}\right|_{T=T_n} = \frac{\epsilon_+(T_n) - \epsilon_-(T_n)}{3w_+(T_n)}, \tag{7}$$

between the false (+) and true (−) vacuums, where $\theta = \epsilon - 3P$ is the trace anomaly, and $w = \epsilon + P$ is the enthalpy. Note that the numerator of (7) is the latent heat for the first-order QCD phase transition at T_n. The effective number of degrees of freedom $g_n = 45s_+/(2\pi^2T_n^3)$. We fix v_w to the typical values $v_w = 0.95$ for which the kinetic energy efficiency coefficient $\kappa = \frac{\alpha}{0.73+0.083\sqrt{\alpha}+\alpha}$. The only free parameter is the inverse time duration of the phase transition β/H_n.

Measurements of primordial element abundances and the anisotropy spectrum of the cosmic microwave background (CMB) yield a strong constraint on the baryon sector, characterized by the baryon asymmetry $\eta_B \equiv n_B/s$.

The observation value $\eta_B^{ob} \approx 10^{-10}$ [69]. This quantity is conserved except during baryogenesis and a first-order phase transition. Thus, to apply to the cosmological QCD phase transition, the baryon asymmetry after the first-order transition in our model should be compatible with η_B^{ob} in the later evolution of the Universe. Near the CEP, our model yields $\eta_B \sim 10^{-2}$, which is eight orders of magnitude larger than the observation. Nevertheless, the value of η_B for the true vacuum at the first-order phase transition line decreases significantly as μ_B increases. In particular, around $\mu_B = 1000$ Mev, η_B reaches the same order of magnitude as the cosmological observation.

We therefore show the GW energy spectrum for $\mu_B = 1000$ Mev ($\mu_B/T \approx 20$) in Fig. 4, for which the cosmological QCD phase transition is first order and does not violate the constraint of a tiny baryon asymmetry. This transition point is very close to the CEP by NJL model [56] (the green triangle at the bottom right of Fig. 3). To account for the uncertainty in the duration β/H_n, we will scan the space with $2 \leq \beta/H_n \leq 80$. The energy density of GWs can reach 10^{-9} around 10^{-7} Hz. While out of reach of the Laser Interferometer Space Antenna (LISA), it can be detected by the International Pulsar Timing Array (IPTA) and the Square Kilometer Array (SKA). The detection from the North American Nanohertz Observatory for Gravitational Wave (NANOGrav) is possible for extreme scenarios with small values of $\beta/H_n \sim \mathcal{O}(1)$.

Moreover, the QCD first-order phase transition with $\mu_B <$ 1000 Mev could also be realized in the early Universe by considering the "little inflation" [71,72] (see e.g., [73–75] for earlier work and the SM). In this scenario, the large baryon asymmetry, which can be generalized by the well-established Affleck-Dine baryogenesis [76] is diluted by a short period of inflation in which the Universe is trapped in a false vacuum state of QCD. We find that the e-folding number sufficient to dilute the baryon number in the little inflation scenario is at most 7. Another scenario for a first-order QCD transition in agreement with observation is to consider a large lepton asymmetry [77,78], which we leave for future work.

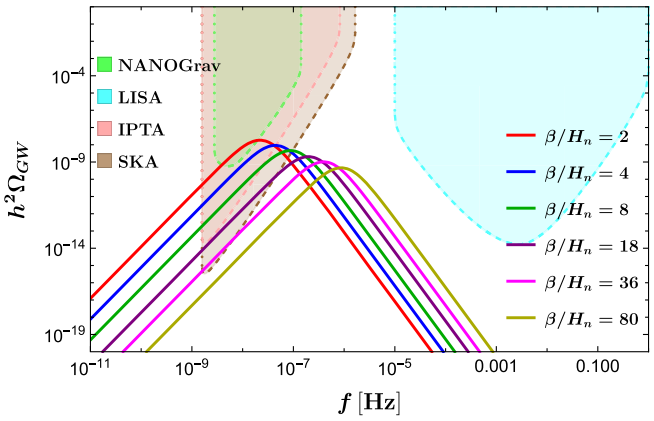

FIG. 4. Stochastic GW spectra predicted from the first-order QCD phase transition at $\mu_B = 1000$ MeV where the baryon asymmetry matches the observation today. Parameters extracted from our holographic model are $(T_n, \alpha, g_n) = (49.53$ MeV, $0.33, 185)$ with the variation of β/H_n. The amplitude of GWs decreases as β/H_n is increased. The sensitivities of four GW detectors (NANOGrav, LISA, IPTA and SKA) are displayed [70].

V. DISCUSSION

We have built a holographic model to confront the phase diagram in $(2+1)$-flavor QCD. The thermodynamics behaviors (EOS, transport, and condensates) are quantitatively matched with the latest lattice QCD simulation. The model has captured the characteristic QCD transition properties and offered a reliable first-order transition line and CEP in the QCD phase diagram at finite μ_B. The predicted location of CEP and the GW energy spectrum of SFOPT from our hQCD model are within the detectivity of upcoming experimental facilities and, therefore, could be verified in the future. Moreover, our EOS at finite density could be crucial for supporting the experimental programs towards QCD matter, e.g., heavy-ion collisions.

Dedicating to a precise characterization of QCD matter, particularly the properties and differences of the quark-gluon plasma and hadronic phases along the first-order phase transition, is an interesting direction for further study. We have set up the preliminary hQCD model to investigate the phase transition in the QCD phase diagram quantitatively. Many other relevant physical quantities should be considered to complete the phase diagram. Moreover, the present study should be embedded in the framework of a more general and multidimensional view of the QCD phase diagram, including magnetic field, isospin, and rotation. It will be interesting to consider real-time dynamics far from equilibrium.

ACKNOWLEDGMENTS

We thank Heng-Tong Ding, Mei Huang, De-Fu Hou, Yi-Bo Yang, Danning Li, Zhibin Li, Shinya Matsuzaki, Shao-Jiang Wang, Yi Yang, Shou-Long Li, and Peihung Yuan for stimulating discussions. This work is supported in part by the National Key Research and Development Program of China Grants No. 2020YFC2201501, No. 2020YFC2201502, and No. 2021YFA0718304, in part by the National Natural Science Foundation of China Grants No. 12075101, No. 12047569, No. 12122513, No. 12075298, No. 11991052, No. 11821505, and No. 12047503, in part by the CAS Project for Young Scientists in Basic Research YSBR-006. S. H. also would like to appreciate the financial support from Jilin University and Max Planck Partner Group.

[1] P. Braun-Munzinger and J. Wambach, The phase diagram of strongly-interacting matter, Rev. Mod. Phys. **81**, 1031 (2009).

[2] O. Philipsen, The QCD equation of state from the lattice, Prog. Part. Nucl. Phys. **70**, 55 (2013).

[3] S. Gupta, X. Luo, B. Mohanty, H. G. Ritter, and N. Xu, Scale for the phase diagram of quantum chromodynamics, Science **332**, 1525 (2011).

[4] S. Borsanyi, G. Endrodi, Z. Fodor, A. Jakovac, S. D. Katz, S. Krieg, C. Ratti, and K. K. Szabo, The QCD equation of state with dynamical quarks, J. High Energy Phys. 11 (2010) 077.

[5] S. Borsanyi, Z. Fodor, C. Hoelbling, S. D. Katz, S. Krieg, and K. K. Szabo, Full result for the QCD equation of state with $2+1$ flavors, Phys. Lett. B **730**, 99 (2014).

[6] A. Bazavov *et al.* (HotQCD Collaboration), Equation of state in $(2+1)$-flavor QCD, Phys. Rev. D **90**, 094503 (2014).

[7] C. R. Allton, S. Ejiri, S. J. Hands, O. Kaczmarek, F. Karsch, E. Laermann, C. Schmidt, and L. Scorzato, The QCD thermal phase transition in the presence of a small chemical potential, Phys. Rev. D **66**, 074507 (2002).

[8] D. Everett *et al.* (JETSCAPE Collaboration), Phenomenological Constraints on the Transport Properties of QCD Matter with Data-Driven Model Averaging, Phys. Rev. Lett. **126**, 242301 (2021).

[9] S. Borsányi, Z. Fodor, J. N. Guenther, R. Kara, S. D. Katz, P. Parotto, A. Pásztor, C. Ratti, and K. K. Szabó, Lattice QCD Equation of State at Finite Chemical Potential from an Alternative Expansion Scheme, Phys. Rev. Lett. **126**, 232001 (2021).

[10] P. Braun-Munzinger, V. Koch, T. Schäfer, and J. Stachel, Properties of hot and dense matter from relativistic heavy ion collisions, Phys. Rep. **621**, 76 (2016).

[11] M. A. Stephanov, QCD phase diagram and the critical point, Prog. Theor. Phys. Suppl. **153**, 139 (2004).

[12] K. Fukushima and C. Sasaki, The phase diagram of nuclear and quark matter at high baryon density, Prog. Part. Nucl. Phys. **72**, 99 (2013).

[13] J. M. Maldacena, The large N limit of superconformal field theories and supergravity, Adv. Theor. Math. Phys. **2**, 231 (1998).

[14] S. S. Gubser, I. R. Klebanov, and A. M. Polyakov, Gauge theory correlators from noncritical string theory, Phys. Lett. B **428**, 105 (1998).

[15] E. Witten, Anti-de Sitter space and holography, Adv. Theor. Math. Phys. **2**, 253 (1998).

[16] E. Witten, Anti-de Sitter space, thermal phase transition, and confinement in gauge theories, Adv. Theor. Math. Phys. **2**, 505 (1998).

[17] S. S. Gubser, A. Nellore, S. S. Pufu, and F. D. Rocha, Thermodynamics and Bulk Viscosity of Approximate Black Hole Duals to Finite Temperature Quantum Chromodynamics, Phys. Rev. Lett. **101**, 131601 (2008).

[18] U. Gursoy, E. Kiritsis, L. Mazzanti, and F. Nitti, Deconfinement and Gluon Plasma Dynamics in Improved Holographic QCD, Phys. Rev. Lett. **101**, 181601 (2008).

[19] M. Panero, Thermodynamics of the QCD Plasma and the Large-N Limit, Phys. Rev. Lett. **103**, 232001 (2009).

[20] M. Järvinen, Holographic modeling of nuclear matter and neutron stars, Eur. Phys. J. C **82**, 282 (2022).

[21] R. Rougemont, J. Noronha, and J. Noronha-Hostler, Suppression of Baryon Diffusion and Transport in a Baryon Rich Strongly Coupled Quark-Gluon Plasma, Phys. Rev. Lett. **115**, 202301 (2015).

[22] O. DeWolfe, S. S. Gubser, and C. Rosen, A holographic critical point, Phys. Rev. D **83**, 086005 (2011).

[23] O. DeWolfe, S. S. Gubser, and C. Rosen, Dynamic critical phenomena at a holographic critical point, Phys. Rev. D **84**, 126014 (2011).

[24] J. Grefa, J. Noronha, J. Noronha-Hostler, I. Portillo, C. Ratti, and R. Rougemont, Hot and dense quark-gluon plasma thermodynamics from holographic black holes, Phys. Rev. D **104**, 034002 (2021).

[25] S. He, S. Y. Wu, Y. Yang, and P. H. Yuan, Phase structure in a dynamical soft-wall holographic QCD model, J. High Energy Phys. 04 (2013) 093.

[26] T. Alho, M. Järvinen, K. Kajantie, E. Kiritsis, C. Rosen, and K. Tuominen, A holographic model for QCD in the Veneziano limit at finite temperature and density, J. High Energy Phys. 04 (2014) 124; 02 (2015) 033(E).

[27] J. Knaute, R. Yaresko, and B. Kämpfer, Holographic QCD phase diagram with critical point from Einstein–Maxwell-dilaton dynamics, Phys. Lett. B **778**, 419 (2018).

[28] R. Critelli, J. Noronha, J. Noronha-Hostler, I. Portillo, C. Ratti, and R. Rougemont, Critical point in the phase diagram of primordial quark-gluon matter from black hole physics, Phys. Rev. D **96**, 096026 (2017).

[29] U. Gursoy, M. Jarvinen, and G. Nijs, Holographic QCD in the Veneziano Limit at a Finite Magnetic Field and Chemical Potential, Phys. Rev. Lett. **120**, 242002 (2018).

[30] Y. Yang and P. H. Yuan, QCD phase diagram by holography, Phys. Lett. B **832**, 137212 (2022).

[31] T. Demircik, C. Ecker, and M. Järvinen, Dense and Hot QCD at Strong Coupling, Phys. Rev. X **12**, 041012 (2022).

[32] R. G. Cai, S. He, and D. Li, A hQCD model and its phase diagram in Einstein-Maxwell-Dilaton system, J. High Energy Phys. 03 (2012) 033.

[33] In most studies, e.g., [24,27,28,30], the thermodynamic variables were obtained by integrating the standard first law of thermodynamics, whose validity is still under investigation for AdS black holes with scalar hair [34–37].

[34] L. Li, On thermodynamics of AdS black holes with scalar hair, Phys. Lett. B **815**, 136123 (2021).

[35] T. Hertog and G. T. Horowitz, Designer Gravity and Field Theory Effective Potentials, Phys. Rev. Lett. **94**, 221301 (2005).

[36] A. Anabalon, D. Astefanesei, D. Choque, and C. Martinez, Trace anomaly and counterterms in designer gravity, J. High Energy Phys. 03 (2016) 117.

[37] H. Lu, C. N. Pope, and Q. Wen, Thermodynamics of AdS black holes in Einstein-scalar gravity, J. High Energy Phys. 03 (2015) 165.

[38] R. G. Cai, Z. Cao, Z. K. Guo, S. J. Wang, and T. Yang, The gravitational-wave physics, Natl. Sci. Rev. **4**, 687 (2017).

[39] C. Caprini, M. Chala, G. C. Dorsch, M. Hindmarsh, S. J. Huber, T. Konstandin, J. Kozaczuk, G. Nardini, J. M. No, K. Rummukainen *et al.*, Detecting gravitational waves from

cosmological phase transitions with LISA: An update, J. Cosmol. Astropart. Phys. 03 (2020) 024.
[40] M. B. Hindmarsh, M. Lüben, J. Lumma, and M. Pauly, Phase transitions in the early universe, Sci. Post Phys. Lect. Notes 24, 1 (2021).
[41] L. Bian, R. G. Cai, S. Cao, Z. Cao, H. Gao, Z. K. Guo, K. Lee, D. Li, J. Liu, Y. Lu *et al.*, The gravitational-wave physics II: Progress, Sci. China Phys. Mech. Astron. 64, 120401 (2021).
[42] K. Skenderis, Lecture notes on holographic renormalization, Classical Quantum Gravity 19, 5849 (2002).
[43] S. de Haro, S. N. Solodukhin, and K. Skenderis, Holographic reconstruction of space-time and renormalization in the AdS/CFT correspondence, Commun. Math. Phys. 217, 595 (2001).
[44] See Supplemental Material at http://link.aps.org/supplemental/10.1103/PhysRevD.106.L121902 for details on the equations of motion, the thermodynamics, the quark and gluon condensates, and the GWs, supporting our statements made in the Letter, which also includes Refs. [79–87].
[45] A. Karch, E. Katz, D. T. Son, and M. A. Stephanov, Linear confinement and AdS/QCD, Phys. Rev. D 74, 015005 (2006).
[46] A. Bazavov, T. Bhattacharya, M. Cheng, N. H. Christ, C. DeTar, S. Ejiri, S. Gottlieb, R. Gupta, U. M. Heller, K. Huebner *et al.*, Equation of state and QCD transition at finite temperature, Phys. Rev. D 80, 014504 (2009).
[47] S. Borsanyi, Z. Fodor, C. Hoelbling, S. D. Katz, S. Krieg, C. Ratti, and K. K. Szabó (Wuppertal-Budapest Collaboration), Is there still any T_c mystery in lattice QCD? Results with physical masses in the continuum limit III, J. High Energy Phys. 09 (2010) 073.
[48] S. Borsanyi, Z. Fodor, S. D. Katz, S. Krieg, C. Ratti, and K. Szabo, Fluctuations of conserved charges at finite temperature from lattice QCD, J. High Energy Phys. 01 (2012) 138.
[49] X. y. Xin, S. x. Qin, and Y. x. Liu, Quark number fluctuations at finite temperature and finite chemical potential via the Dyson-Schwinger equation approach, Phys. Rev. D 90, 076006 (2014).
[50] F. Gao and Y. x. Liu, QCD phase transitions via a refined truncation of Dyson-Schwinger equations, Phys. Rev. D 94, 076009 (2016).
[51] S. x. Qin, L. Chang, H. Chen, Y. x. Liu, and C. D. Roberts, Phase Diagram and Critical Endpoint for Strongly-Interacting Quarks, Phys. Rev. Lett. 106, 172301 (2011).
[52] C. Shi, Y. L. Wang, Y. Jiang, Z. F. Cui, and H. S. Zong, Locate QCD critical end point in a continuum model study, J. High Energy Phys. 07 (2014) 014.
[53] C. S. Fischer, J. Luecker, and C. A. Welzbacher, Phase structure of three and four flavor QCD, Phys. Rev. D 90, 034022 (2014).
[54] F. Gao and J. M. Pawlowski, QCD phase structure from functional methods, Phys. Rev. D 102, 034027 (2020).
[55] Z. Li, K. Xu, X. Wang, and M. Huang, The kurtosis of net baryon number fluctuations from a realistic Polyakov–Nambu–Jona-Lasinio model along the experimental freeze-out line, Eur. Phys. J. C 79, 245 (2019).
[56] M. Asakawa and K. Yazaki, Chiral restoration at finite density and temperature, Nucl. Phys. A504, 668 (1989).
[57] W. j. Fu, J. M. Pawlowski, and F. Rennecke, QCD phase structure at finite temperature and density, Phys. Rev. D 101, 054032 (2020).
[58] H. Zhang, D. Hou, T. Kojo, and B. Qin, Functional renormalization group study of the quark-meson model with ω meson, Phys. Rev. D 96, 114029 (2017).
[59] J. Adam *et al.* (STAR Collaboration), Nonmonotonic Energy Dependence of Net-Proton Number Fluctuations, Phys. Rev. Lett. 126, 092301 (2021).
[60] K. Fukushima, B. Mohanty, and N. Xu, Little-Bang and femto-nova in nucleus-nucleus collisions, AAPPS Bull. 31, 1 (2021).
[61] M. A. Stephanov, K. Rajagopal, and E. V. Shuryak, Event-by-event fluctuations in heavy ion collisions and the QCD critical point, Phys. Rev. D 60, 114028 (1999).
[62] A. Bazavov, H. T. Ding, P. Hegde, O. Kaczmarek, F. Karsch, E. Laermann, Y. Maezawa, S. Mukherjee, H. Ohno, P. Petreczky *et al.*, The QCD equation of state to $\mathcal{O}(\mu_B^6)$ from lattice QCD, Phys. Rev. D 95, 054504 (2017).
[63] T. Ablyazimov *et al.* (CBM Collaboration), Challenges in QCD matter physics–The scientific programme of the Compressed Baryonic Matter experiment at FAIR, Eur. Phys. J. A 53, 60 (2017).
[64] M. Durante, P. Indelicato, B. Jonson, V. Koch, K. Langanke, U. G. Meißner, E. Nappi, T. Nilsson, T. Stöhlker, E. Widmann *et al.*, All the fun of the FAIR: Fundamental physics at the facility for antiproton and ion research, Phys. Scr. 94, 033001 (2019).
[65] A. N. Sissakian, and A. S. Sorin (NICA Collaboration), The nuclotron-based ion collider facility (NICA) at JINR: New prospects for heavy ion collisions and spin physics, J. Phys. G 36, 064069 (2009).
[66] S. L. Li, L. Shao, P. Wu, and H. Yu, NANOGrav signal from first-order confinement-deconfinement phase transition in different QCD-matter scenarios, Phys. Rev. D 104, 043510 (2021).
[67] D. Bodeker and G. D. Moore, Electroweak bubble wall speed limit, J. Cosmol. Astropart. Phys. 05 (2017) 025.
[68] H. K. Guo, K. Sinha, D. Vagie, and G. White, The benefits of diligence: How precise are predicted gravitational wave spectra in models with phase transitions?, J. High Energy Phys. 06 (2021) 164.
[69] N. Aghanim *et al.* (Planck Collaboration), Planck 2018 results. VI. Cosmological parameters, Astron. Astrophys. 641, A6 (2020); 652, C4(E) (2021).
[70] K. Schmitz, New sensitivity curves for gravitational-wave signals from cosmological phase transitions, J. High Energy Phys. 01 (2021) 097.
[71] T. Boeckel and J. Schaffner-Bielich, A Little Inflation in the Early Universe at the QCD Phase Transition, Phys. Rev. Lett. 105, 041301 (2010); 106, 069901(E) (2011).
[72] T. Boeckel and J. Schaffner-Bielich, A little inflation at the cosmological QCD phase transition, Phys. Rev. D 85, 103506 (2012).
[73] A. D. Linde, The new mechanism of baryogenesis and the inflationary universe, Phys. Lett. 160B, 243 (1985).

[74] B. Kampfer, Entropy production during an isothermal phase transition in the early Universe, Astron. Nachr. **307**, 231 (1986).
[75] N. Borghini, W. N. Cottingham, and R. V. Mau, Possible cosmological implications of the quark-hadron phase transition, J. Phys. G **26**, 771 (2000).
[76] I. Affleck and M. Dine, A new mechanism for baryogenesis, Nucl. Phys. **B249**, 361 (1985).
[77] D. J. Schwarz and M. Stuke, Lepton asymmetry and the cosmic QCD transition, J. Cosmol. Astropart. Phys. 11 (2009) 025; 10 (2010) E01.
[78] F. Gao and I. M. Oldengott, Cosmology Meets Functional QCD: First-Order Cosmic QCD Transition Induced by Large Lepton Asymmetries, Phys. Rev. Lett. **128**, 131301 (2022).
[79] E. Kiritsis and L. Li, Holographic competition of phases and superconductivity, J. High Energy Phys. 01 (2016) 147.
[80] R. G. Cai, L. Li, and R. Q. Yang, No inner-horizon theorem for black holes with charged scalar hairs, J. High Energy Phys. 03 (2021) 263.
[81] A. Bazavov, T. Bhattacharya, M. Cheng, C. DeTar, H. T. Ding, S. Gottlieb, R. Gupta, P. Hegde, U. M. Heller, F. Karsch *et al.*, The chiral and deconfinement aspects of the QCD transition, Phys. Rev. D **85**, 054503 (2012).
[82] P. Gubler and D. Satow, Recent progress in QCD condensate evaluations and sum rules, Prog. Part. Nucl. Phys. **106**, 1 (2019).
[83] M. A. Shifman, A. I. Vainshtein, and V. I. Zakharov, Remarks on Higgs boson interactions with nucleons, Phys. Lett. **78B**, 443 (1978).
[84] T. D. Cohen, R. J. Furnstahl, and D. K. Griegel, Quark and gluon condensates in nuclear matter, Phys. Rev. C **45**, 1881 (1992).
[85] D. d'Enterria, S. Kluth, S. Alekhin, P. A. Baikov, A. Banfi, F. Barreiro, A. Bazavov, S. Bethke, J. Blümlein, D. Boito *et al.*, $\alpha_s(2019)$: Precision measurements of the QCD coupling, arXiv:1907.01435.
[86] A. I. Alekseev, Strong coupling constant to four loops in the analytic approach to QCD, Few Body Syst. **32**, 193 (2003).
[87] J. A. M. Vermaseren, S. A. Larin, and T. van Ritbergen, The four loop quark mass anomalous dimension and the invariant quark mass, Phys. Lett. B **405**, 327 (1997).